Heliyon 10 (2024) e25691

Contents lists available at ScienceDirect

Heliyon

journal homepage: www.cell.com/heliyon

Research article

Construction of molecular subtype model of osteosarcoma based on endoplasmic reticulum stress and tumor metastasis-related genes

Wang-Qiang Wu [a], Cheng-Da Zou [b], Di Wu [a], Hou-Xin Fu [a], Xiao-Dong Wang [a], Feng Yao [a,*]

[a] Department of Orthopaedics, Children's Hospital of Soochow University, 92# Zhongnan Street, Suzhou, Jiangsu 215025, China
[b] Children's Hospital of Soochow University, Children's Hospital of Wujiang District, China

ARTICLE INFO

Keywords:
Osteosarcoma
Metastasis
Endoplasmic reticulum stress
Subtype analysis

ABSTRACT

Introduction: Osteosarcoma, the prevailing primary bone malignancy among children and adolescents, is frequently associated with treatment failure primarily due to its pronounced metastatic nature.

Methods: This study aimed to establish potential associations between hub genes and subtypes for the treatment of metastatic osteosarcoma. Differentially expressed genes were extracted from patients diagnosed with metastatic osteosarcoma and a control group of non-metastatic patients, using the publicly available gene expression profile (GSE21257). The intersection of these gene sets was determined by focusing on endoplasmic reticulum (ER) stress-related genes sourced from the GeneCards database. We conducted various analytical techniques, including functional and pathway enrichment analysis, WGCNA analysis, protein-protein interaction (PPI) network construction, and assessment of immune cell infiltration, using the intersecting genes. Through this analysis, we identified potential hub genes.

Results: Osteosarcoma subtype models were developed using molecular consensus clustering analysis, followed by an examination of the associations between each subtype and hub genes. A total of 138 potential differentially expressed genes related to endoplasmic reticulum (ER) stress were identified. These genes were further investigated using Gene Ontology (GO), Kyoto Encyclopedia of Genes and Genomes (KEGG), and Gene Set Enrichment Analysis (GSEA) pathways. Additionally, the PPI interaction network revealed 38 interaction relationships among the top ten hub genes. The findings of the analysis revealed a strong correlation between the extent of immune cell infiltration and both osteosarcoma metastasis and the expression of hub genes. Notably, the differential expression of the top ten hub genes was observed in osteosarcoma clusters 1 and 4, signifying their significant association with the disease.

Conclusion: The identification of ten key genes linked to osteosarcoma metastasis and endoplasmic reticulum stress bears potential clinical significance. Additionally, exploring the molecular subtype of osteosarcoma has the capacity to guide clinical treatment decisions, necessitating further investigations and subsequent clinical validations.

* Corresponding author.
E-mail addresses: wwq809607955@163.com (W.-Q. Wu), zcdqwe12@163.com (C.-D. Zou), waynewu629@126.com (D. Wu), 71337402@qq.com (H.-X. Fu), wangxd@suda.edu.cn (X.-D. Wang), felixyao@suda.edu.cn (F. Yao).

https://doi.org/10.1016/j.heliyon.2024.e25691
Received 8 February 2023; Received in revised form 24 January 2024; Accepted 31 January 2024
Available online 6 February 2024

1. Introduction

Osteosarcoma, a primary bone tumor prevalent among children and adolescents, exhibits an annual incidence of approximately 8–11/million [1]. This malignancy is characterized by its highly aggressive nature, heterogeneity, and propensity for metastasis [2], leading to a significant risk of disability and mortality following metastatic spread. Osteosarcoma commonly manifests in the vicinity of the metaphysis of long bones, including the distal femur, proximal tibia, and humerus [3]. The precise etiology, progression, and metastasis of osteosarcoma have not been thoroughly investigated [4,5]. However, the elevated prevalence among adolescents and its predilection for specific anatomical sites suggest a correlation with accelerated bone tissue growth [6]. Presently, the primary therapeutic approach for osteosarcoma entails preoperative chemotherapy, surgical excision, and postoperative chemotherapy. Despite extensive removal of macroscopic tumor tissue during surgical intervention, recurrence frequently occurs [7]. The implementation of neoadjuvant chemotherapy has led to a substantial enhancement in the 5-year survival rate among individuals diagnosed with osteosarcoma [8]. When neoadjuvant chemotherapy is combined with surgical resection, the 5-year survival rate for patients with non-metastatic osteosarcoma is approximately 60% [9]. However, the survival rate drops significantly to only 20–30% for patients with metastatic osteosarcoma [9–11]. The high incidence of metastasis in osteosarcoma is the primary determinant of the unfavorable prognosis [12]. Presently, there is no treatment available that significantly improves the 5-year survival rate for patients with metastatic osteosarcoma [13].

The endoplasmic reticulum (ER) plays a crucial role in the processes of protein synthesis, folding, and structural maturation. ER stress, which occurs as a result of genetic or environmental factors, disrupts the ER's ability to properly modify, fold, and secrete proteins, leading to the accumulation of misfolded proteins within organelles [14]. This phenomenon of ER stress is closely linked to the onset and progression of various diseases, including tumors, diabetes, and neurodegenerative disorders [15–17]. Unfavorable conditions within the tumor microenvironment, including nutritional deficiency, hypoxia, hypermetabolism, and oxidative stress, have been shown to disrupt protein folding by the endoplasmic reticulum (ER), leading to the persistent activation of "ER stress." This phenomenon enhances the tumorigenic, metastatic, and drug-resistant properties of malignant cells [14,16,18]. Osteosarcoma is characterized by extensive genetic variation, dysregulation of multiple signaling pathways, and genome instability. These factors are closely associated with the regulation of bone development, tumor microenvironment, genome homeostasis, cell cycle control, and cell signal transduction pathways [16]. The correlation between ER stress-related genes and osteosarcoma metastasis has been established [19], and the utilization of molecular subtype models is crucial for predicting tumor risk and evaluating prognosis [20–22]. Nevertheless, there is currently a lack of research on molecular subtype models specifically pertaining to ER stress and osteosarcoma metastasis.

In this study, the author developed a molecular subtype model for osteosarcoma AMI. By analyzing the gene data from 14 metastatic osteosarcoma patients and 19 non-metastatic osteosarcoma patients, the study identified co-expressed differential genes associated with osteosarcoma metastasis and ER stress. Subsequently, a validation set comprising 10 key genes was established, confirming the robustness of the molecular subtype model for osteosarcoma. These key genes hold promise as potential targets for targeted therapeutic drugs and molecular markers for prognostic evaluation.

2. Materials and methods

1 GEO data difference analysisC

We performed an analysis on the osteosarcoma dataset. GSE21257 comes from the Gene Expression Omnibus (GEO) database [23]. GSE21257 has 53 samples, including 14 samples of osteosarcoma metastases (metastases present at diagnosis) and 19 samples of non-metastases (no metastases). The chip platform is a GPL10295 Illumina human-6 v2. 0 expression beadchip (using nuIDs as identifiers).

We used the standardized data expression matrix downloaded from GEO to match, select, and delete gene data based on the samples. The selected samples were grouped according to metastasis and non-metastasis for subsequent analysis. For the preprocessed data set, we drew a boxplot using the R language's boxplot function to observe the data distribution. Expression difference *P*-values and expression fold change values were calculated using the R package limma (Version 3.42.2) [24]. We selected genes with a *P*-value <0.05 and $|\log2FC| > 0.263$ (1.2-fold relationship) as significantly differentially expressed mRNAs. The R package heatmap function (Version 1.0.12) [25] was used to make differential heat maps and volcano maps for visualization.

2 Molecular subtype construction

We calculated the AMI molecular subtypes with the ConsensusClusterPlus package [26] and the Rtsne package [27]. The ggplot2 package was used for molecular subtype visualization. Correlations between hub genes and molecular subtypes were plotted with the gspubr package.

3 Enrichment analysis of intersection genes

The GeneCards database (https://www.genecards.org/) [28] provides annotated and predicted human genetic information. The database automatically integrated genetic data from approximately 150 network sources, including genomics, transcriptomics,

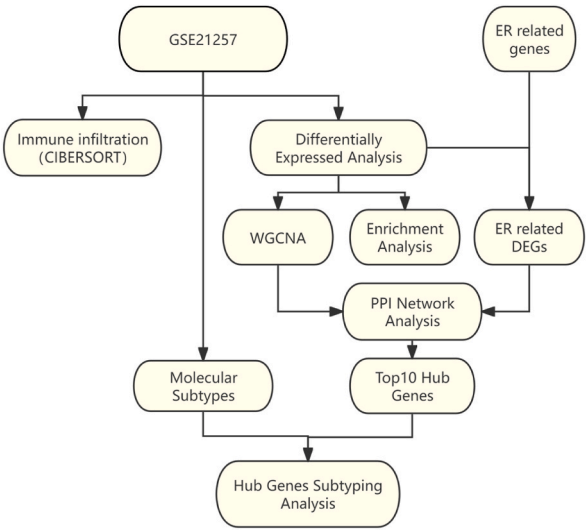

Fig. 1. Flow chart.

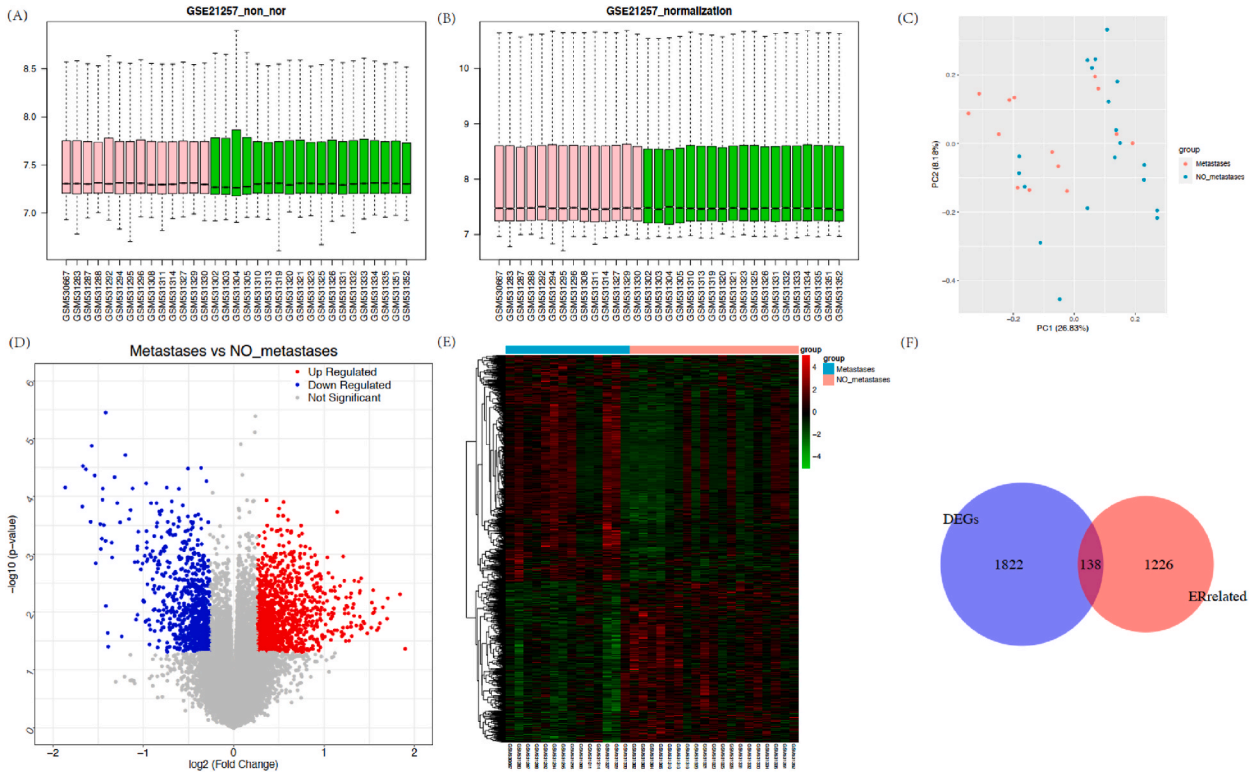

Fig. 2. Difference analysis (Pink is the metastatic group and green is the non-metastatic group): **(A) Boxplot before GSE21257 data processing. (B) Boxplots after GSE21257 data processing. (C) PCA graph. (D)GSE21257 dataset differential genes volcano plot.** Red is up-regulated differential genes, blue is down-regulated differential genes, and grey is non-significant genes. **(E) GSE21257 datasetdifferential genes heat map.** Blue is the metastatic group, pink is the non-metastatic group, green is low expression, and red is high expression. **(F) Venn diagram of the intersection of endoplasmic reticulum stress-related genes and differential genes.** 138 potential ER stress-related differentially expressed genes. (For interpretation of the references to color in this figure legend, the reader is referred to the Web version of this article.)

2 Molecular Subtype Construction

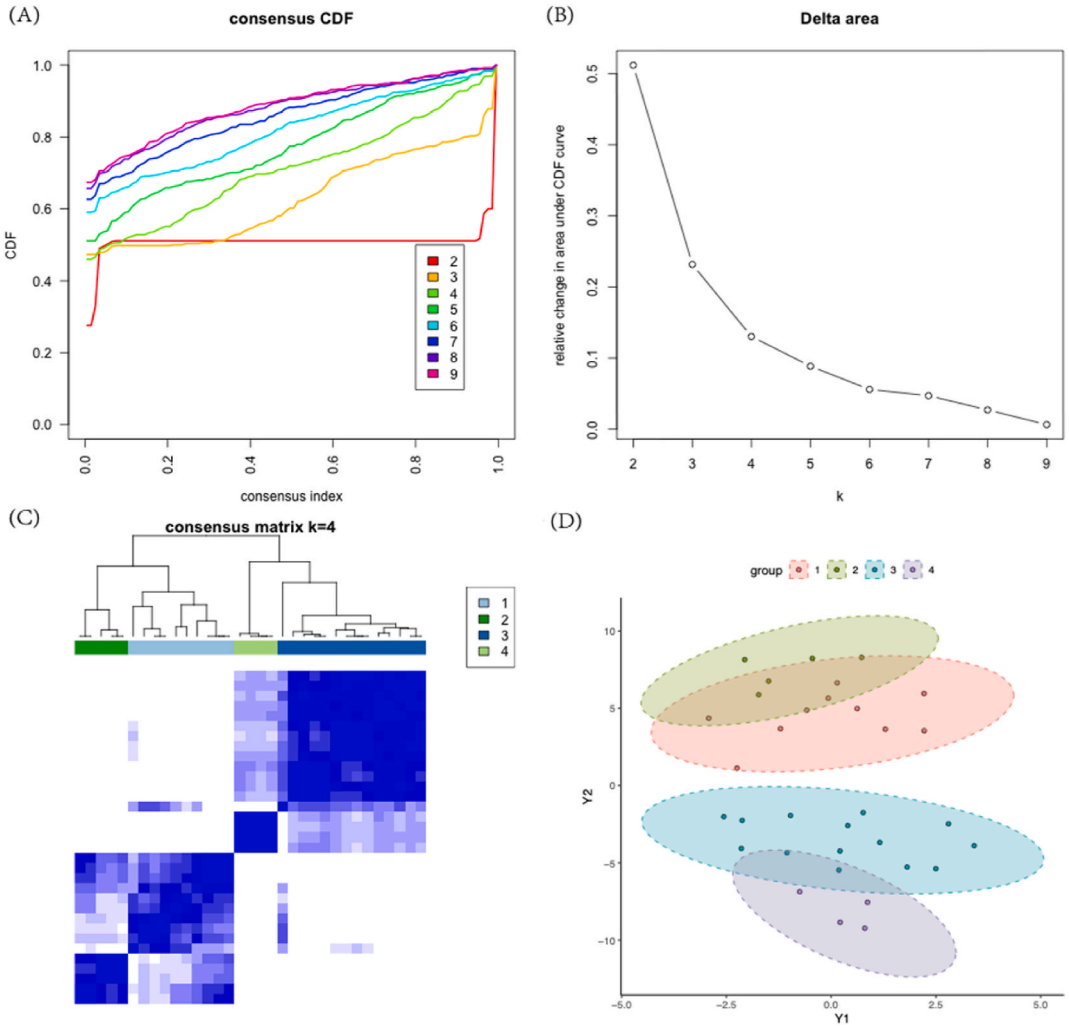

Fig. 3. Molecular typing of osteosarcoma: (A) The cumulative distribution function (CDF) curve. (B) The CDF Delta area curve. (C) Heat map of molecular subtype sample clustering. (D) The spatial distribution of different clusters.

3 Enrichment analysis

proteomics, and genetics, as well as clinical and functional information.

In this analysis, ER stress-related genes were downloaded from the GeneCards database using "endoplasmic reticulum stress" as the search key. We took the intersection of differential genes and ER stress-related human genes to create a Venn diagram, which was constructed using the R-package Venn diagram function (Version 1.6.20) [29].

Gene Ontology (GO) [30] describes our understanding of the field of biology based on three aspects, molecular function (MF), cellular components (CC), and biological processes (BP). GO enrichment analysis is typically used to explore the enrichment degree of GO terms associated with differentially expressed genes. Kyoto Encyclopedia of Genes and Genomes (KEGG) [31] is a utility database resource for understanding advanced functions and biological systems (such as cells, organisms, and ecosystems) based on molecular-level information, especially genome sequencing and other high-throughput experimental techniques generated from large molecular datasets. KEGG was established in 1995 by Kanehisa's laboratory at the Center for Bioinformatics at Kyoto University, Japan.

The analysis used in this study was based on the use of the R package clusterProfiler package (version 3.14.3) [32] to perform GO function/pathway enrichment analysis on the intersection genes and the significance threshold was set to $P \leq 0.05$. Bubble plots were created for visualization using the R package ggplot2 (Version 3.3.3) [33]. The pathway network diagram was drawn to visualize the pathway relationship using the cytoscape plug-in ClueGo [34].

We selected and downloaded the c2.cp.v7.2.symbols.gmt gene set data from the GSEA (http://www.gsea-msigdb.org/gsea/index.jsp) [35] database as the reference gene set and performed GSEA enrichment analysis on the two sets of data with the R clusterProfiler package. The GSEA statistical process was used to calculate the enrichment score, estimate the significance of the enrichment score, correct for multiple hypothesis testing, and select the enrichment results with $P < 0.05$ to draw the GSEA enrichment map.

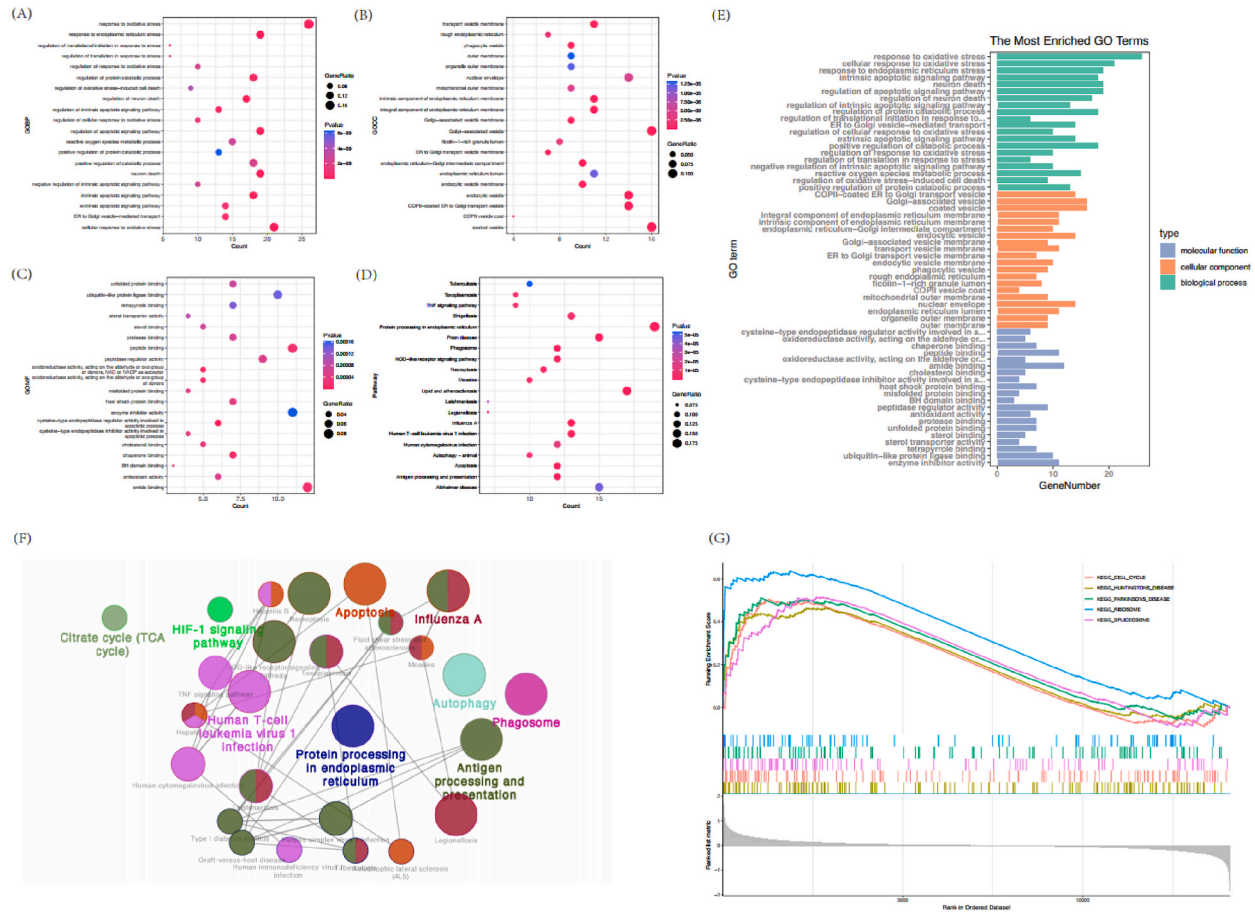

Fig. 4. Enrichment analysis: (A) GOBP enrichment bubble chart of intersection genes. The vertical axis is the BP name, the horizontal axis is the number of enriched genes, and the dot size is the ratio of the number of enriched genes to the total number of uploaded genes. The larger the ratio, the larger the dots. The redder the dot color, the more significant the P value. **(B) GOCC enrichment bubble chart of intersection genes.** The vertical axis is the CC name, the horizontal axis is the number of enriched genes, and the size of the dots is the ratio of the number of enriched genes to the total number of uploaded genes. The larger the ratio, the larger the dots. The redder the dot color, the more significant the P value. **(C) GOMF enrichment bubble chart of intersection genes.**The vertical axis is the MF name, the horizontal axis is the number of enriched genes, and the size of the dots is the ratio of the number of enriched genes to the total number of uploaded genes. The larger the ratio, the larger the dots. The redder the dot color, the more significant the P value. **(D) PathwaysEnrichment bubble chart of intersection genes.** The vertical axis is the pathways name, the horizontal axis is the number of enriched genes, and the size of the dots is the ratio of the number of enriched genes to the total number of uploaded genes. The larger the ratio, the larger the dots. The redder the dot color, the more significant the P value. **(E) GO enrichment histogram of intersection genes.** The horizontal axis is the number of genes, and the vertical axis is the GO item. **(F) KEGG network diagram.** Different colors represent different types of KEGG pathways, and bold fonts represent pathways.The more significant the P value, the larger the dots, and the two-point line represents the correlation between functions. **(G) TOP5 KEGG GSEA diagram.** Enrichment Score polyline section.The horizontal axis is the sorted gene, and the vertical axis is the corresponding ES.The peak in the line graph is the Enrichment score of this genes set, and the genes before the peak are the core genes under the genes set. (For interpretation of the references to color in this figure legend, the reader is referred to the Web version of this article.)

4 WGCNA analysis

4 WGCNA analysis

The gene co-expression network was constructed using the WGCNA R package [36]. By calculating the Pearson correlation coefficient between two genes, we used the expression data to create a similarity matrix and chose an appropriate soft threshold β to make the constructed network more compatible with the standard of a scale-free network. We transformed the adjacency matrix into a topological overlap matrix TOM and used hierarchical clustering to generate a hierarchical clustering tree of genes. The correlations between genes and clinical information were calculated, and the significant associations of modules with ER-related DEGs were analyzed.

5 PPI Interaction Network Construction

Table 1
GO enrichment.

ID	Type	Description	pvalue
GO:0006979	BP	response to oxidative stress	2.66E-16
GO:0034599	BP	cellular response to oxidative stress	6.49E-15
GO:0034976	BP	response to endoplasmic reticulum stress	2.97E-13
GO:0097193	BP	intrinsic apoptotic signaling pathway	4.12E-12
GO:0070997	BP	neuron death	1.01E-11
GO:2001233	BP	regulation of apoptotic signaling pathway	1.42E-10
GO:1901214	BP	regulation of neuron death	1.45E-10
GO:2001242	BP	regulation of intrinsic apoptotic signaling pathway	2.58E-10
GO:0042176	BP	regulation of protein catabolic process	3.88E-10
GO:0043558	BP	regulation of translational initiation in response to stress	4.00E-10
GO:0006888	BP	ER to Golgi vesicle-mediated transport	5.34E-10
GO:1900407	BP	regulation of cellular response to oxidative stress	9.02E-10
GO:0097191	BP	extrinsic apoptotic signaling pathway	1.10E-09
GO:0009896	BP	positive regulation of catabolic process	2.05E-09
GO:1902882	BP	regulation of response to oxidative stress	2.38E-09
GO:0043555	BP	regulation of translation in response to stress	2.41E-09
GO:2001243	BP	negative regulation of intrinsic apoptotic signaling pathway	2.63E-09
GO:0072593	BP	reactive oxygen species metabolic process	2.75E-09
GO:1903201	BP	regulation of oxidative stress-induced cell death	3.94E-09
GO:0045732	BP	positive regulation of protein catabolic process	6.27E-09
GO:0030134	CC	COPII-coated ER to Golgi transport vesicle	3.20E-15
GO:0005798	CC	Golgi-associated vesicle	1.27E-13
GO:0030135	CC	coated vesicle	2.02E-10
GO:0030176	CC	integral component of endoplasmic reticulum membrane	8.59E-09
GO:0031227	CC	intrinsic component of endoplasmic reticulum membrane	1.48E-08
GO:0005793	CC	endoplasmic reticulum-Golgi intermediate compartment	1.96E-08
GO:0030139	CC	endocytic vesicle	2.90E-08
GO:0030660	CC	Golgi-associated vesicle membrane	1.08E-07
GO:0030658	CC	transport vesicle membrane	2.47E-07
GO:0012507	CC	ER to Golgi transport vesicle membrane	2.52E-07
GO:0030666	CC	endocytic vesicle membrane	2.82E-07
GO:0045335	CC	phagocytic vesicle	3.80E-07
GO:0005791	CC	rough endoplasmic reticulum	2.21E-06
GO:1904813	CC	ficolin-1-rich granule lumen	2.61E-06
GO:0030127	CC	COPII vesicle coat	2.95E-06
GO:0005741	CC	mitochondrial outer membrane	4.59E-06
GO:0005635	CC	nuclear envelope	4.84E-06
GO:0005788	CC	endoplasmic reticulum lumen	1.15E-05
GO:0031968	CC	organelle outer membrane	1.23E-05
GO:0019867	CC	outer membrane	1.33E-05
GO:0043028	MF	cysteine-type endopeptidase regulator activity involved in apoptotic process	8.04E-07
GO:0016620	MF	oxidoreductase activity, acting on the aldehyde or oxo group of donors, NAD or NADP as acceptor	6.96E-06
GO:0051087	MF	chaperone binding	1.43E-05
GO:0042277	MF	peptide binding	1.89E-05
GO:0016903	MF	oxidoreductase activity, acting on the aldehyde or oxo group of donors	1.96E-05
GO:0033218	MF	amide binding	2.13E-05
GO:0015485	MF	cholesterol binding	3.75E-05
GO:0043027	MF	cysteine-type endopeptidase inhibitor activity involved in apoptotic process	3.83E-05
GO:0031072	MF	heat shock protein binding	3.89E-05
GO:0051787	MF	misfolded protein binding	4.50E-05
GO:0051400	MF	BH domain binding	5.23E-05
GO:0061134	MF	peptidase regulator activity	5.26E-05
GO:0016209	MF	antioxidant activity	5.46E-05
GO:0002020	MF	protease binding	6.20E-05
GO:0051082	MF	unfolded protein binding	7.18E-05
GO:0032934	MF	sterol binding	7.19E-05
GO:0015248	MF	sterol transporter activity	9.19E-05
GO:0046906	MF	tetrapyrrole binding	0.00013578
GO:0044389	MF	ubiquitin-like protein ligase binding	0.00014405
GO:0004857	MF	enzyme inhibitor activity	0.00016315

*Only top 20 BP,CC, MF were displayed.

The STRING (version 11.0, http://www.string-db.org/) database [37] was used to perform protein-protein interactions (PPI) on critical module genes from the WGCNA results and the ER stress-related differentially expressed genes. We selected Required Confidence (combined score) > 0.4 as the threshold value of the PPI relationship. Cytoscape software [38] was used to construct the PPI network of interaction genes, and the top ten hub genes were extracted using the cytohbhs plug-in Ref. [39].

Table 2
KEGG enrichment.

ID	Description	pvalue	gene
hsa04141	Protein processing in endoplasmic reticulum	8.78E-14	PRKCSH/TRAM1/RPN2/AMFR/GANAB/CANX/RBX1/UBQLN2/SEC24D/HSPA6/ATF4/DNAJC1/EIF2S1/DNAJC10/EIF2AK2/SEC23B/HSPA1A/SAR1A/SEC23A
hsa04612	Antigen processing and presentation	9.66E-11	HLA-DRA/CD74/TNF/HSPA4/IFNG/CANX/HSPA6/TAP1/CTSB/TAP2/HLA-B/HSPA1A
hsa05417	Lipid and atherosclerosis	4.84E-10	TNF/CYBB/BAD/TLR4/HSPA4/BCL2L1/IL1B/HSPA6/ATF4/PIK3CA/SOD2/APAF1/EIF2S1/CYBA/HSPA1A/OLR1/ABCA1
hsa04210	Apoptosis	6.40E-08	TNF/BAD/MCL1/BCL2L1/ACTG1/ATF4/PIK3CA/APAF1/EIF2S1/ACTB/BIRC2/CTSB
hsa05164	Influenza A	1.03E-07	HLA-DRA/VDAC1/TNF/TLR4/IFNG/IL1B/KPNA2/ACTG1/PIK3CA/APAF1/EIF2S1/ACTB/EIF2AK2
hsa04145	Phagosome	2.19E-07	HLA-DRA/CYBB/TLR4/ACTG1/CANX/ACTB/CYBA/PIK3C3/TAP1/TAP2/HLA-B/OLR1
hsa05020	Prion disease	7.09E-07	VDAC1/TNF/CYBB/CREB3L1/SDHC/BAD/IL1B/HSPA6/ATF4/PIK3CA/APAF1/EIF2S1/CYBA/HSPA1A/ATF2
hsa04621	NOD-like receptor signaling pathway	1.72E-06	VDAC1/TNF/DNM1L/CYBB/TLR4/BCL2L1/IL1B/TXNIP/BIRC2/CYBA/CTSB/GABARAP
hsa05166	Human T-cell leukemia virus 1 infection	2.07E-06	HLA-DRA/VDAC1/TNF/CREB3L1/BCL2L1/CANX/MYC/ATF4/PIK3CA/IL1R1/PTEN/HLA-B/ATF2
hsa04217	Necroptosis	2.70E-06	VDAC1/TNF/DNM1L/CYBB/GLUD1/TLR4/IFNG/IL1B/HMGB1/EIF2AK2/BIRC2
hsa05134	Legionellosis	4.56E-06	TNF/TLR4/IL1B/HSPA6/APAF1/HSPA1A/SAR1A
hsa05162	Measles	5.57E-06	BAD/TLR4/BCL2L1/IL1B/HSPA6/PIK3CA/APAF1/EIF2S1/EIF2AK2/HSPA1A
hsa04140	Autophagy - animal	6.33E-06	BAD/BCL2L1/HMGB1/PIK3CA/PTEN/EIF2S1/PIK3C3/CTSB/ATG7/GABARAP
hsa05131	Shigellosis	6.74E-06	VDAC1/TNF/TLR4/BCL2L1/IL1B/UBC/ACTG1/RBX1/PXN/PIK3CA/IL1R1/ACTB/PIK3C3
hsa04668	TNF signaling pathway	6.83E-06	TNF/DNM1L/CREB3L1/IL1B/ATF4/PIK3CA/BIRC2/CEBPB/ATF2
hsa05145	Toxoplasmosis	6.83E-06	HLA-DRA/TNF/BAD/TLR4/BCL2L1/IFNG/HSPA6/BIRC2/HSPA1A
hsa05163	Human cytomegalovirus infection	1.37E-05	TNF/CREB3L1/IL1B/MYC/ATF4/PXN/PIK3CA/IL1R1/TAP1/TAP2/HLA-B/ATF2
hsa05140	Leishmaniasis	3.41E-05	HLA-DRA/TNF/CYBB/TLR4/IFNG/IL1B/CYBA
hsa05010	Alzheimer disease	4.50E-05	VDAC1/TNF/CYBB/SDHC/BAD/IL1B/APOE/ATF4/PIK3CA/APAF1/EIF2S1/EIF2AK2/SNCA/PIK3C3/GAPDH
hsa05152	Tuberculosis	5.33E-05	HLA-DRA/CD74/TNF/BAD/TLR4/IFNG/IL1B/APAF1/PIK3C3/CEBPB

*Only top 20 items were displayed.

6 Analysis of Immune Cell Infiltration

CIBERSORT is based on the principle of linear support vector regression to deconvolve the transcriptome expression matrix and estimate the composition and abundance of immune cells in mixed cell populations [40]. We used the gene expression matrix data to analyze the infiltration of 22 immune genes in the samples using the CIBERSORT algorithm. The samples with $P < 0.05$ were filtered to obtain the immune cell infiltration matrix. The corplot package [41] was used to draw correlation heatmaps to visualize the correlations of the 22 immune cell infiltrations. The gepubr package (https:/CRAN.R-pnojiect.org/package-ggpuby) was used to draw violin plots to visualize the differences in the infiltration of the 22 immune cells. We plotted the correlations between the hub genes and immune cells.

7 Statistical analysis

All statistical analyses were performed using means ± standard deviation. The data were analyzed using R software (version 3.6.3). A *P*-value <0.05 was considered statistically significant, and all statistical tests were two-sided. The overall analysis protocol used in this study is shown in Fig. 1.

3. Results

1 GEO data variance analysis

The downloaded standardized data was preprocessed to obtain a boxplot of the data before and after preprocessing (Fig. 2A and B). The results of the PCA analysis revealed specific differences between the metastatic and non-metastatic groups (Fig. 2C). The

Table 3
GSEA Enrichment results.

Description	ES	NES	p-val
huntingtons disease	0.46630952	1.58440333	0.00172712
cell cycle	0.50538946	1.64173798	0.00177936
spliceosome	0.51580512	1.62686146	0.00177936
parkinsons disease	0.51169624	1.61820978	0.00178891
ribosome	0.63942248	1.9899259	0.00179211
asthma	−0.8866284	−2.3835054	0.00204499
primary immunodeficiency	−0.6713973	−1.8398342	0.00205761
allograft rejection	−0.845997	−2.3734866	0.00208768
type i diabetes mellitus	−0.7803001	−2.2486644	0.0021097
nod like receptor signaling pathway	−0.7042556	−2.0714756	0.00212766
graft versus host disease	−0.8501564	−2.4277465	0.0021322
cytosolic dna sensing pathway	−0.6094253	−1.7984544	0.00214592
systemic lupus erythematosus	−0.8388346	−2.488651	0.00214592
autoimmune thyroid disease	−0.8391577	−2.4826173	0.00215054
intestinal immune network for iga production	−0.822676	−2.3955756	0.00215054
viral myocarditis	−0.7628128	−2.379273	0.00215983
b cell receptor signaling pathway	−0.5974895	−1.8628274	0.00218818
toll like receptor signaling pathway	−0.6431166	−2.1193684	0.00220264
complement and coagulation cascades	−0.7051765	−2.1764987	0.00220751
leishmania infection	−0.789533	−2.4331695	0.00221239
cell adhesion molecules cams	−0.6483611	−2.2007646	0.00223214
natural killer cell mediated cytotoxicity	−0.6285108	−2.1406363	0.00224719
lysosome	−0.5284886	−1.7686821	0.00228833
hematopoietic cell lineage	−0.6706642	−2.1650725	0.00230415
antigen processing and presentation	−0.7504096	−2.4231959	0.00231481
chemokine signaling pathway	−0.5715468	−2.0123182	0.00236967
cytokine cytokine receptor interaction	−0.5242236	−1.9269993	0.00239234
jak stat signaling pathway	−0.4284559	−1.4716202	0.00473934
ubiquitin mediated proteolysis	0.45041173	1.49145857	0.00714286

*Only top 20 items were displayed.

GSE21257 data set screened the expression data for 24,994 genes with $|\log FC|>0.263$, p.adj<0.05 as the threshold. Finally, 1960 differentially expressed genes were identified, of which 1145 were up-regulated and 815 were down-regulated (Fig. 2D and E). The ER stress-related genes were downloaded from the GeneCard database. Then, 138 potential ER stress-related differentially expressed genes were identified by their intersection with the previously detected differentially expressed genes from the GSE21257 data set (Fig. 2F).

We used the consensus clustering method to cluster the samples. In the CDF curve of the consensus matrix, when K = 4, the CDF curve presented a relatively flat middle segment (Fig. 3A and B). Furthermore, when K = 4 was selected for consensus clustering analysis, the interference between subgroups was reduced considerably (Fig. 3C). Therefore, we identified four subgroups, including cluster 1 (n = 10), cluster 2 (n = 5), cluster 3 (n = 14), and cluster 4 (n = 4). The expression profiles between the four clusters were compared (Fig. 3D).

As described in the methods, the 138 intersection genes were subjected to enrichment analysis, including 1337 significant items for biological processes (BP), 116 significant items for cellular components (CC), 86 significant items for molecular function (MF), and 112 significant pathways. The significant items were displayed using bubble charts (Fig. 4A–D). As shown in Fig. 4 below, the BP, CC, and MF items revealed the top 20 items based on the *P*-value (Fig. 4E–Table 1). It was noted that the differentially expressed genes related to ER stress-affected pathways such as Protein processing in the ER, Apoptosis, and Antigen processing and presentation (Fig. 4F–Table 2). Based on the GSEA analysis, the GSE21257 data set had 29 significant gene set pathways (Table 3), and the TOP5 pathways included Huntington's disease, cell cycle, the spliceosome, Parkinson's disease, and ribosomes (Fig. 4G).

We performed a weighted gene co-expression network analysis (WGCNA) on the gene expression data using the R package WGCNA algorithm to identify the co-expression patterns of the genes during osteosarcoma metastasis. First, we performed sample clustering analysis to detect any variation across the 35 samples and outliers. Next, we set a soft threshold of 3 to approximate the network to a scale-free network (Fig. 5A). Then, the Pearson correlation coefficient of paired genes was calculated to obtain a similarity matrix. The similarity matrix was transformed into an adjacent matrix using the threshold and power values listed above. Linkage hierarchical clustering was then averaged to identify the modules where genes were closely linked, and genes not assigned to a specific module were shown in grey (Fig. 5B). We found one module of significantly co-expressed genes (MEblue, $P = 0.01$) (Fig. 5C). The identified genes were closely associated with osteosarcoma metastasis, suggesting that this was a critical gene set to investigate the risk of osteosarcoma metastasis further (Fig. 5D).

The PPI interaction network analysis was performed on the ER stress-related differentially expressed genes (Fig. 6A) in the 81 blue modules. As shown in Fig. 6B and C, there were 218 interaction relationships among 68 key genes, and there were 38 interaction relationships among the top ten critical genes, as seen in Fig. 6D.

The CIBERSORT algorithm was used to assess changes in immune cell infiltration levels before and after osteosarcoma metastasis as described in the Methods (Fig. 7A and B). The results of the correlation analysis revealed a positive correlation between osteosarcoma

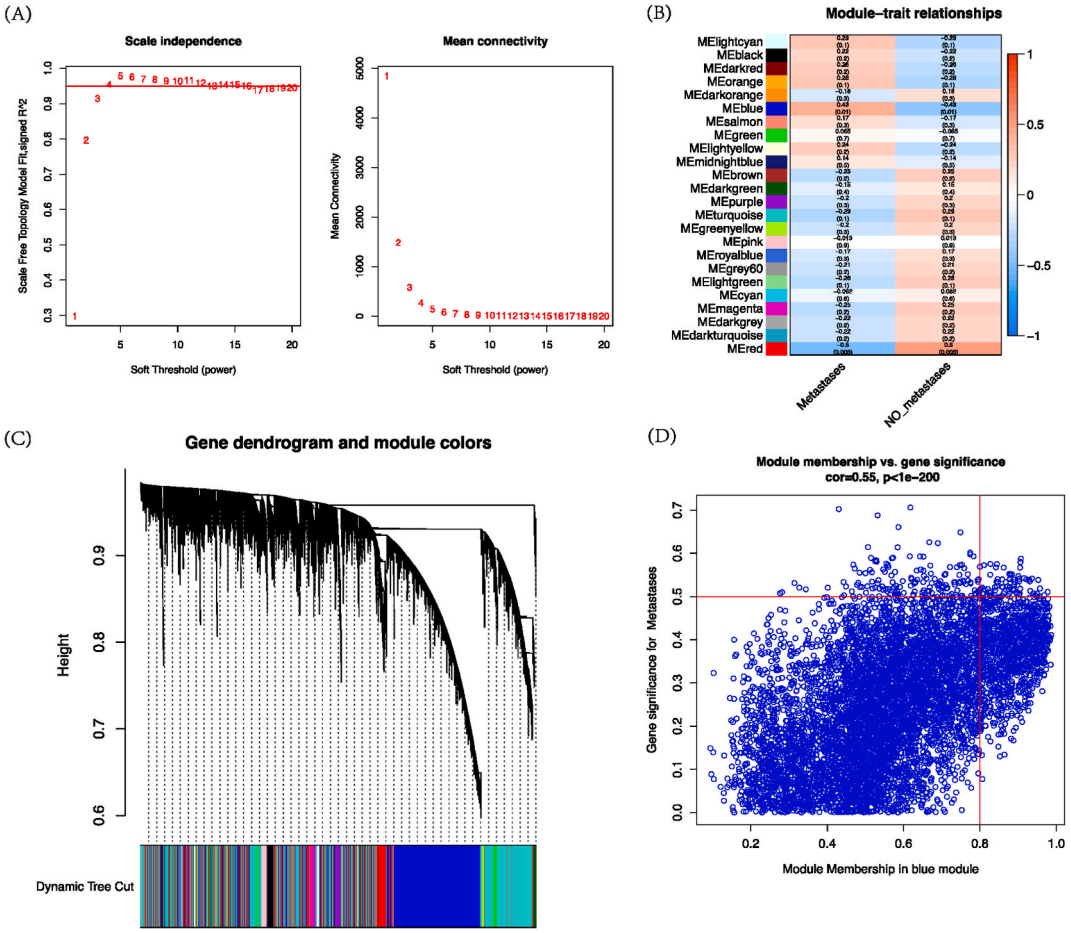

Fig. 5. WGCNA analysis: (A) Soft Threshold. (B) Module and Trait Data Heatmap. Orange means positive correlation, blue means negative correlation, the darker the color, the stronger the correlation. **(C)Module Clustering Plot. (D)Blue Significant Difference Module Scatter Plot**. (For interpretation of the references to color in this figure legend, the reader is referred to the Web version of this article.)

5 PPI Interaction Network

metastasis and the infiltration levels of various immune cells, such as naive CD4 T cells and neutrophils (Fig. 7C). A negative correlation was observed for other immune cells such as CD8 T cells and M0 macrophages. The differential analysis demonstrated that the infiltration levels of various immune cell subsets were significantly different between the metastatic and non-metastatic groups (Fig. 7D), including M0 macrophages, CD8 T cells, and others. The correlation analysis showed that the expression of hub genes was primarily related to memory B cells, CD4 T cells, memory resting, and others (Fig. 7E-N).

To elucidate the immune microenvironmental status of these four subgroups, we explored the expression of ten Hub genes across the four clusters. All ten genes were significantly differentially expressed in clusters 1 and 4 (Fig. 8A–J).

4. Discussion

ER stress has been found to be associated with the incidence, progression, spread, and resistance to drugs of tumors [14,16,18]. Once the accumulation of improperly folded proteins in the ER surpasses a crucial threshold, it triggers a signal transduction pathway known as the unfolded protein response (UPR). The heightened activation of UPR signaling is implicated in the epithelial-mesenchymal transition (EMT) of tumor cells preceding metastasis [16]. The UPR is initiated by three ER transmembrane proteins: PERK, IRE1α, and ATF6 [15]. The up-regulation of LAMP3 by PERK has been shown to facilitate the migration and invasion of cancer cells [42]. Tumor metastasis is closely associated with the epithelial-mesenchymal transformation (EMT) process in tumor cells [4,43]. Inhibition of the EMT process through small-molecule PERK inhibitors has been found to effectively suppress the migration of tumor cells [44]. Additionally, IRE1α and ATF6 play significant roles in regulating various physiological and pathological processes in different cell types [45–47].

In this study, the author searched for a set of differentially expressed genes associated with ER stress and osteosarcoma metastasis. Through bioinformatics analysis of gene data of 14 metastatic osteosarcoma patients and 19 non-metastatic patients, enrichment

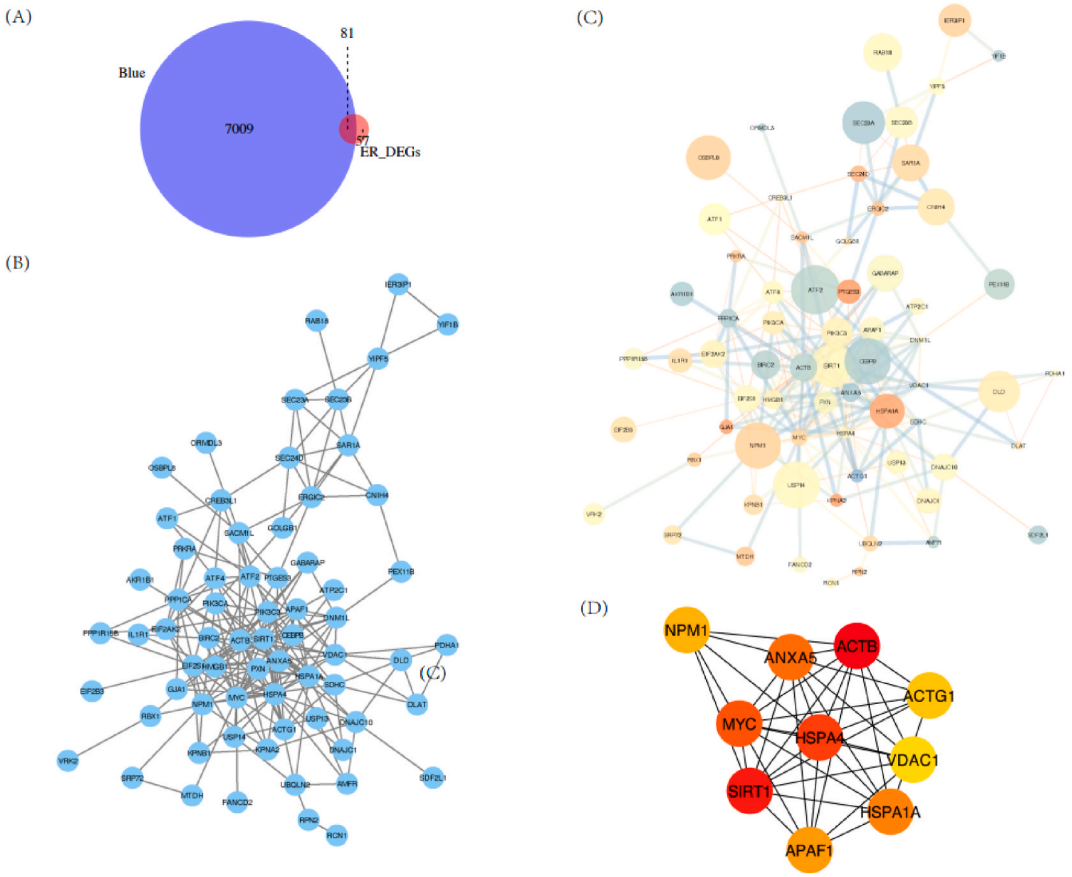

Fig. 6. PPI interaction analysis of key genes: (A) Venn diagram of the intersection of ER stress-related differential genes and key genes in the blue module. (B) PPI interaction network diagram The blue dots are key genes, and the connectionsare interactions. **(C) PPI interaction NetworkAnalyzer visualization.** The smaller the significance, the larger the dots are.The thickness of edge is the combine score, and the color is down-regulated to up-regulated from blue to red. **(D) Hub gene interaction diagram.** The color from red to light is the MCC score. (For interpretation of the references to color in this figure legend, the reader is referred to the Web version of this article.)

6 Immune infiltration correlation analysis

analysis, immune infiltration analysis, PPI protein interaction network analysis of differentially expressed genes associated with ER stress, construction and verification of a molecular subtype model related to metastatic osteosarcoma, 10 key genes were finally determined, namely ACTB, ACTG1, ANXA5, APAF1, HSPA1A, HSPA4, MYC, NPM1, SIRT1 and VDAC1, providing possibility for inhibiting the occurrence of osteosarcoma metastasis. ACTB, also known as β-actin (ACTB), plays a crucial role in cancer metastasis, particularly in liver cancer [43]. The processes of polymerization, localization, cytoskeleton formation, and overexpression of ACTB are closely associated with cell growth and migration [43,48]. In the context of prostate cancer (PCa), ACTG1 may impact tumor metastasis through the MAPK/ERK signaling pathway [49]. Additionally, Annexin ANXA5 serves as a link between the innate and adaptive immune systems and contributes to immune stimulation within the tumor microenvironment (TME). ANXA5-carbon nanotube conjugates have been utilized for the physical ablation of tumors through photothermal therapy [50]. Apoptosis protease activating factor-1 (APAF-1), a protein weighing 130 kDa, plays a crucial role in regulating programmed cell death. In metastatic colorectal cancer, the frequent absence of APAF-1 expression is strongly linked to unfavorable prognosis. Furthermore, the loss of APAF-1 expression is more prevalent among patients experiencing early recurrence, emphasizing its significance in tumor metastasis [51]. HSPA1A plays a crucial role in facilitating the proper folding of recently synthesized proteins and inhibiting the aggregation of pre-existing proteins within the cytoplasm and organelles. In the context of squamous cell carcinoma, HSPA1A exhibits a direct binding affinity and interaction with LASP1, thereby effectively stimulating the proliferation, metastasis, and invasion of malignant cells [52]. In hepatocellular carcinoma (HCC), the downregulation of HSPA1A, HSPA4, and VDAC1 has been found to impede the invasion, migration, and proliferation of HCC cells [53,54]. Additionally, HSPA1A, HSPA4, and VDAC1 have been identified as independent prognostic factors. The inhibition of miR-93b expression by MYC through direct binding to the promoter region of miR-193b, along with the indirect inhibition of MYC expression by miR-194b, suggests that miR-193b may exhibit an anti-tumor effect on osteosarcoma by targeting KRAS and STMN1. The reciprocal negative regulatory loop involving MYC and miR-93b potentially leads to a persistent upregulation of MYC and downregulation of miR-193b, subsequently leading to enhanced expression of KRAS and

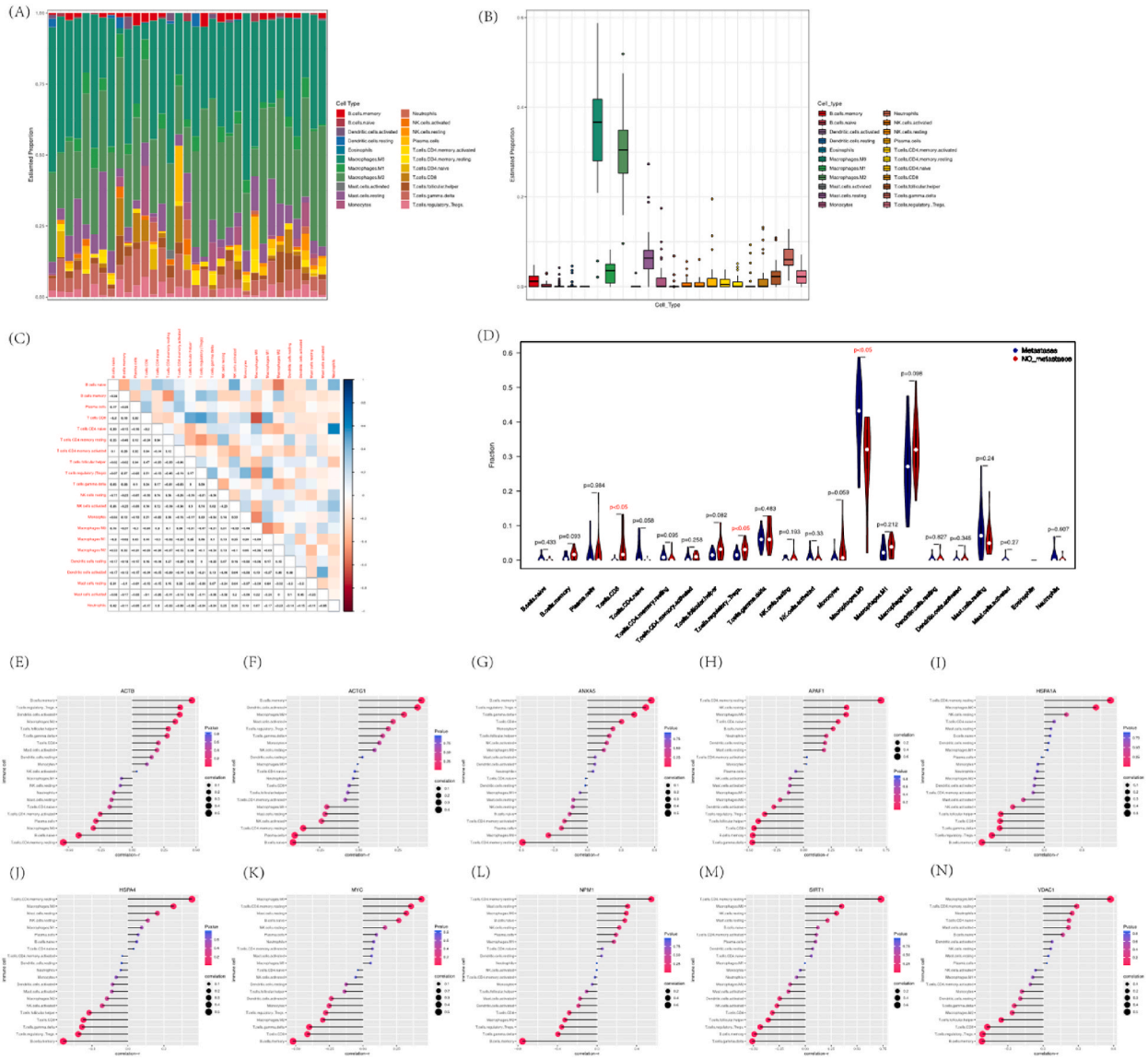

Fig. 7. Analysis of immune infiltration: (A) Histogram of immune infiltration distribution. The horizontal axis is the cell type, and the vertical axis is the estimated proportion. **(B) Histogram of the distribution of immune infiltration samples**.The horizontal axis is the sample, the vertical axis is the estimated proportion, and different colors represent different immune cells. **(C) Heat map related with immune infiltration.** Correlation of cellular immune infiltration in each sample, positive correlation in blue, negative correlation in red. **(D) Violin plot of the correlation of cellular immune infiltration between the metastatic group and the non-metastatic group.** The horizontal axis is the type of immune cells, the vertical axis is the cell immune infiltration score, the blue is the metastatic group, the red is the non-metastatic group. **(E–N) Bar graph related with hub genes immune infiltration**. The horizontal axis is the correlation score, and the vertical axis is the immune cell type. The size of the dots is the correlation, the higher the correlation, the larger the dots. The redder the color, the more significant the *P* value. (For interpretation of the references to color in this figure legend, the reader is referred to the Web version of this article.)

7 Correlation analysis between Hub genes and different molecular subtypes

STMN1, ultimately culminating in the development and metastasis of osteosarcoma. Suppression of MYC expression has been demonstrated to effectively impede osteosarcoma metastasis [55]. In vitro experiments involving the treatment of osteosarcoma cell lines KHOS and U2OS with the MYC inhibitor 10058-F4 resulted in a significant reduction in migration distance [56]. The NPM1/ERK/NF-κβ pathway has been found to facilitate the growth and metastasis of osteosarcoma, with NPM1 identified as a crucial molecule in this process [57]. Sirtuin-1 (SIRT1), a class III histone deacetylase, is extensively implicated in gene regulation, genome stability maintenance, apoptosis, autophagy, aging, proliferation, and tumor metastasis [58,59]. SIRT1 plays a pivotal role in governing the proliferation and metastasis of cancer cells under stress by modulating p53-dependent aging and cell reprogramming [60]. Furthermore, it has been determined that the aforementioned 10 crucial genes exhibit a strong correlation with the degree of immune

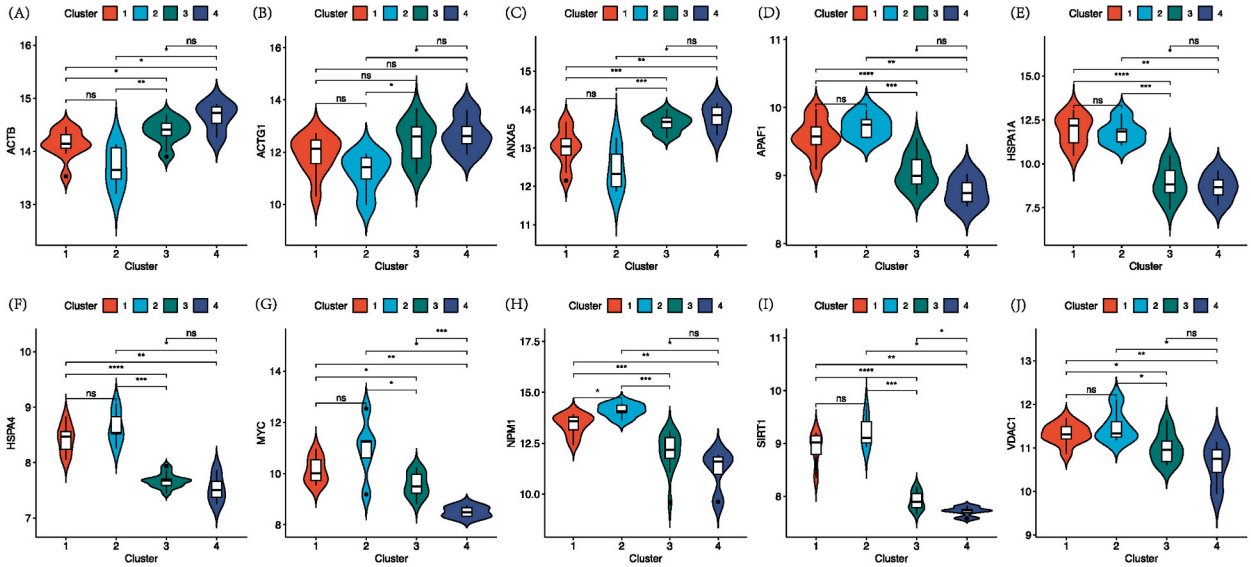

Fig. 8. Correlation diagram between Hub genes and different molecular subtypes **(A–J) Violin plots of correlation between different molecular subtypes and hub genes**.

cell infiltration and the immune microenvironment. The researcher effectively utilized these genes to validate the molecular subtype model of osteosarcoma. Notably, there was a significant disparity in the expression of these 10 pivotal molecules between cluster 1 and cluster 4, underscoring the potential of the molecular subtype model to facilitate the categorization of osteosarcoma patients and provide valuable guidance for personalized therapeutic interventions [61]. The ten identified genes are anticipated to serve as molecular markers for distinguishing between metastatic and non-metastatic osteosarcoma. Furthermore, these genes hold potential for identifying osteosarcoma micrometastasis and osteosarcoma with a pronounced propensity for extensive metastasis, pending further development and application.

Inhibiting osteosarcoma metastasis is a reliable scheme to improve the cure rate of osteosarcoma. Early prevention of osteosarcoma metastasis is expected to improve the cure rate of osteosarcoma. In this study, 10 key genes associated with ER stress and osteosarcoma metastasis were identified, but the results lack further clinical validation, and the involved cell signaling pathways have not been further validated in vivo and in vitro. The study primarily adopts an observational approach, thus it does not establish causal relationships between ER stress and osteosarcoma metastasis. Additional experimental studies are required to validate the mechanistic connections between these phenomena. Nonetheless, this study successfully constructs a molecular subtype model of osteosarcoma using bioinformatics methods and identifies key molecules, thereby offering significant scientific and potential clinical value.

5. Conclusion

The identification of 10 key genes associated with osteosarcoma metastasis and ER stress holds potential clinical significance. Furthermore, the molecular subtype of osteosarcoma has the potential to inform clinical treatment decisions However, further investigations and future clinical validations are necessary to establish the identified key genes and their correlations definitively.

Funding

This study was supported by Suzhou Municipal Health Commission (KJXW2022017) and Children's Hospital of Soochow University Youth Project (2021QN04).

Ethics approval and consent to participate

Not applicable.

Consent for publication

Not applicable.

CRediT authorship contribution statement

Wang-Qiang Wu: Data curation. **Cheng-Da Zou:** Writing – original draft. **Di Wu:** Formal analysis. **Hou-Xin Fu:** Software. **Xiao-Dong Wang:** Supervision, Funding acquisition. **Feng Yao:** Writing – review & editing, Writing – original draft, Funding acquisition.

Declaration of competing interest

The authors declare that they have no known competing financial interests or personal relationships that could have appeared to influence the work reported in this paper.

Acknowledgements

We thank Home for Researchers editorial team (www.home-for-researchers.com)for language editing service.

References

[1] L. Mirabello, R.J. Troisi, S.A. Savage, Osteosarcoma incidence and survival rates from 1973 to 2004: data from the surveillance, epidemiology, and end results program, Cancer 115 (7) (2009) 1531–1543, https://doi.org/10.1002/cncr.24121.
[2] A. Smrke, P.M. Anderson, A. Gulia, S. Gennatas, P.H. Huang, R.L. Jones, Future directions in the treatment of osteosarcoma, Cells 10 (1) (2021) 172, https://doi.org/10.3390/cells10010172.
[3] X. Huang, J. Zhao, J. Bai, H. Shen, B. Zhang, L. Deng, C. Sun, Y. Liu, J. Zhang, J. Zheng, Risk and clinicopathological features of osteosarcoma metastasis to the lung: a population-based study, J Bone Oncol 16 (2019 Mar 7) 100230, https://doi.org/10.1016/j.jbo.2019.100230.
[4] G. Sheng, Y. Gao, Y. Yang, H. Wu, Osteosarcoma and metastasis, Frontiers in oncology 11 (2021) 780264, https://doi.org/10.3389/fonc.2021.780264.
[5] A.M. Czarnecka, K. Synoradzki, W. Firlej, E. Bartnik, P. Sobczuk, M. Fiedorowicz, P. Grieb, P. Rutkowski, Molecular biology of osteosarcoma, Cancers 12 (8) (2020) 2130, https://doi.org/10.3390/cancers12082130.
[6] L. Mirabello, R.J. Troisi, S.A. Savage, International osteosarcoma incidence patterns in children and adolescents, middle ages and elderly persons, International journal of cancer 125 (1) (2009) 229–234, https://doi.org/10.1002/ijc.24320.
[7] J. Ritter, S.S. Bielack, Osteosarcoma, Annals of oncology : official journal of the European Society for Medical Oncology 21 (Suppl 7) (2010) vii320–vii325, https://doi.org/10.1093/annonc/mdq276.
[8] Y. Jiang, F. Li, B. Gao, M. Ma, M. Chen, Y. Wu, W. Zhang, Y. Sun, S. Liu, H. Shen, KDM6B-mediated histone demethylation of LDHA promotes lung metastasis of osteosarcoma, Theranostics 11 (8) (2021) 3868–3881, https://doi.org/10.7150/thno.53347.
[9] J. Zhang, N. Li, S. Lu, Y. Chen, L. Shan, X. Zhao, Y. Xu, The role of Notch ligand Jagged1 in osteosarcoma proliferation, metastasis, and recurrence, Journal of orthopaedic surgery and research 16 (1) (2021) 226, https://doi.org/10.1186/s13018-021-02372-y.
[10] F. Duffaud, Role of TKI for metastatic osteogenic sarcoma, Current treatment options in oncology 21 (8) (2020) 65, https://doi.org/10.1007/s11864-020-00760-w.
[11] F. Yao, Z.F. Zhu, J. Wen, F.Y. Zhang, Z. Zhang, L.Q. Zhu, G.H. Su, Q.W. Yuan, Y.F. Zhen, X.D. Wang, PODN is a prognostic biomarker and correlated with immune infiltrates in osteosarcoma, Cancer cell international 21 (1) (2021) 381, https://doi.org/10.1186/s12935-021-02086-5.
[12] K.H. Lu, R.C. Lin, J.S. Yang, W.E. Yang, R.J. Reiter, S.F. Yang, Molecular and cellular mechanisms of melatonin in osteosarcoma, Cells 8 (12) (2019) 1618, https://doi.org/10.3390/cells8121618.
[13] R. Belayneh, M.S. Fourman, S. Bhogal, K.R. Weiss, Update on osteosarcoma, Current oncology reports 23 (6) (2021) 71, https://doi.org/10.1007/s11912-021-01053-7.
[14] L. Cheng, T. Chen, M. Guo, P. Liu, X. Qiao, Y. Wei, J. She, B. Li, W. Xi, J. Zhou, Z. Yuan, Y. Wu, J. Liu, Glycoursodeoxycholic acid ameliorates diet-induced metabolic disorders with inhibiting endoplasmic reticulum stress, Clinical science (London, England : 1979) 135 (14) (2021) 1689–1706, https://doi.org/10.1042/CS20210198.
[15] R. Ghemrawi, M. Khair, Endoplasmic reticulum stress and unfolded protein response in neurodegenerative diseases, International journal of molecular sciences 21 (17) (2020) 6127, https://doi.org/10.3390/ijms21176127.
[16] S.A. Oakes, Endoplasmic reticulum stress signaling in cancer cells, The American journal of pathology 190 (5) (2020) 934–946, https://doi.org/10.1016/j.ajpath.2020.01.010.
[17] S. Mustapha, M. Mohammed, A.K. Azemi, A.I. Jatau, A. Shehu, L. Mustapha, I.M. Aliyu, R.N. Danraka, A. Amin, A.A. Bala, W. Ahmad, A. Rasool, M.R. Mustafa, S.S. Mokhtar, Current status of endoplasmic reticulum stress in type II diabetes, Molecules (Basel, Switzerland) 26 (14) (2021) 4362, https://doi.org/10.3390/molecules26144362.
[18] J.R. Cubillos-Ruiz, S.E. Bettigole, L.H. Glimcher, Tumorigenic and immunosuppressive effects of endoplasmic reticulum stress in cancer, Cell 168 (4) (2017) 692–706, https://doi.org/10.1016/j.cell.2016.12.004.
[19] I. Lilienthal, N. Herold, Targeting molecular mechanisms underlying treatment efficacy and resistance in osteosarcoma: a review of current and future strategies, International journal of molecular sciences 21 (18) (2020) 6885, https://doi.org/10.3390/ijms21186885.
[20] H. Wang, H. Liu, L. Wang, S. Xu, H. Pi, Z. Cheng, Subtype classification and prognosis signature construction of osteosarcoma based on cellular senescence-related genes, J Oncol (2022) 4421952, https://doi.org/10.1155/2022/4421952. Sep 5;2022.
[21] J. Hong, Q. Li, X. Wang, J. Li, W. Ding, H. Hu, L. He, Development and validation of apoptosis-related signature and molecular subtype to improve prognosis prediction in osteosarcoma patients, J Clin Lab Anal 36 (7) (2022 Jul) e24501, https://doi.org/10.1002/jcla.24501. Epub 2022 May 16.
[22] C. Dong, Y. Sun, Y. Zhang, B. Qin, T. Lei, Construction of molecular subtype and prognosis prediction model of osteosarcoma based on aging-related genes, J Oncol (2022) 8177948, https://doi.org/10.1155/2022/8177948. Sep 16;2022.
[23] T. Barrett, S.E. Wilhite, P. Ledoux, C. Evangelista, I.F. Kim, M. Tomashevsky, K.A. Marshall, K.H. Phillippy, P.M. Sherman, M. Holko, A. Yefanov, H. Lee, N. Zhang, C.L. Robertson, N. Serova, S. Davis, A. Soboleva, NCBI GEO: archive for functional genomics data sets–update, Nucleic acids research 41 (2013) D991–D995, https://doi.org/10.1093/nar/gks1193. Database issue.
[24] G.K. Smyth, Limma: linear models for microarray data, in: R. Gentleman, V.J. Carey, W. Huber, R.A. Irizarry, S. Dudoit (Eds.), Bioinformatics and Computational Biology Solutions Using R and Bioconductor. Statistics for Biology and Health, Springer, New York, NY, 2005, https://doi.org/10.1007/0-387-29362-0_23.
[25] Raivo Kolde, Pheatmap: Pretty Heatmaps. R Package, 2019 version 1.0.12, https://CRAN.R-project.org/package=pheatmap.
[26] M.D. Wilkerson, D.N. Hayes, ConsensusClusterPlus: a class discovery tool with confidence assessments and item tracking, Bioinformatics (Oxford, England) 26 (12) (2010) 1572–1573, https://doi.org/10.1093/bioinformatics/btq170.
[27] Jesse H. Krijthe, Rtsne: T-distributed stochastic neighbor embedding using a barnes-hut implementation. https://github.com/jkrijthe/Rtsne, 2015.
[28] G. Stelzer, N. Rosen, I. Plaschkes, S. Zimmerman, M. Twik, S. Fishilevich, T.I. Stein, R. Nudel, I. Lieder, Y. Mazor, S. Kaplan, D. Dahary, D. Warshawsky, Y. Guan-Golan, A. Kohn, N. Rappaport, M. Safran, D. Lancet, The GeneCards suite: from gene data mining to disease genome sequence analyses, Current protocols in bioinformatics 54 (2016) 1–30, https://doi.org/10.1002/cpbi.5.
[29] Hanbo Chen, VennDiagram: Generate High-Resolution Venn and Euler Plots, 2018. R package version 1.6.20, https://CRAN.R-project.org/package=VennDiagram.

[30] M. Ashburner, C.A. Ball, J.A. Blake, D. Botstein, H. Butler, J.M. Cherry, A.P. Davis, K. Dolinski, S.S. Dwight, J.T. Eppig, M.A. Harris, D.P. Hill, L. Issel-Tarver, A. Kasarskis, S. Lewis, J.C. Matese, J.E. Richardson, M. Ringwald, G.M. Rubin, G. Sherlock, Gene ontology: tool for the unification of biology. The Gene Ontology Consortium, Nature genetics 25 (1) (2000) 25–29, https://doi.org/10.1038/75556.

[31] M. Kanehisa, S. Goto, KEGG: kyoto encyclopedia of genes and genomes, Nucleic acids research 28 (1) (2000) 27–30, https://doi.org/10.1093/nar/28.1.27.

[32] G. Yu, L.G. Wang, Y. Han, Q.Y. He, clusterProfiler: an R package for comparing biological themes among gene clusters, Omics : a journal of integrative biology 16 (5) (2012) 284–287, https://doi.org/10.1089/omi.2011.0118.

[33] H. Wickham, ggplot2: Elegant Graphics for Data Analysis, Springer-Verlag New York, 2016, 2016, https://link.springer.com/content/pdf/10.1007%2F978-3-319-24277-4.pdf.

[34] G. Bindea, B. Mlecnik, H. Hackl, P. Charoentong, M. Tosolini, A. Kirilovsky, W.H. Fridman, F. Pagès, Z. Trajanoski, J. Galon, ClueGO: a Cytoscape plug-in to decipher functionally grouped gene ontology and pathway annotation networks, Bioinformatics (Oxford, England) 25 (8) (2009) 1091–1093, https://doi.org/10.1093/bioinformatics/btp101.

[35] A. Subramanian, P. Tamayo, V.K. Mootha, S. Mukherjee, B.L. Ebert, M.A. Gillette, A. Paulovich, S.L. Pomeroy, T.R. Golub, E.S. Lander, J.P. Mesirov, Gene set enrichment analysis: a knowledge-based approach for interpreting genome-wide expression profiles, Proceedings of the National Academy of Sciences of the United States of America 102 (43) (2005) 15545–15550, https://doi.org/10.1073/pnas.0506580102.

[36] P. Langfelder, S. Horvath, WGCNA: an R package for weighted correlation network analysis, BMC bioinformatics 9 (2008) 559, https://doi.org/10.1186/1471-2105-9-559.

[37] D. Szklarczyk, A.L. Gable, D. Lyon, A. Junge, S. Wyder, J. Huerta-Cepas, M. Simonovic, N.T. Doncheva, J.H. Morris, P. Bork, L.J. Jensen, C.V. Mering, STRING v11: protein-protein association networks with increased coverage, supporting functional discovery in genome-wide experimental datasets, Nucleic acids research 47 (D1) (2019) D607–D613, https://doi.org/10.1093/nar/gky1131.

[38] P. Shannon, A. Markiel, O. Ozier, N.S. Baliga, J.T. Wang, D. Ramage, N. Amin, B. Schwikowski, T. Ideker, Cytoscape: a software environment for integrated models of biomolecular interaction networks, Genome research 13 (11) (2003) 2498–2504, https://doi.org/10.1101/gr.1239303.

[39] C.H. Chin, S.H. Chen, H.H. Wu, C.W. Ho, M.T. Ko, C.Y. Lin, cytoHubba: identifying hub objects and sub-networks from complex interactome, BMC systems biology 8 (Suppl 4) (2014), https://doi.org/10.1186/1752-0509-8-S4-S11. Suppl 4), S11.

[40] A.M. Newman, C.L. Liu, M.R. Green, A.J. Gentles, W. Feng, Y. Xu, C.D. Hoang, M. Diehn, A.A. Alizadeh, Robust enumeration of cell subsets from tissue expression profiles, Nature methods 12 (5) (2015) 453–457, https://doi.org/10.1038/nmeth.3337.

[41] Taiyun Wei, Viliam Simko, R Package "corrplot": Visualization of a Correlation Matrix, 2017, Version 0.84.

[42] H. Mujcic, A. Nagelkerke, K.M. Rouschop, S. Chung, N. Chaudary, P.N. Span, B. Clarke, M. Milosevic, J. Sykes, R.P. Hill, M. Koritzinsky, B.G. Wouters, Hypoxic activation of the PERK/eIF2α arm of the unfolded protein response promotes metastasis through induction of LAMP3, Clinical cancer research : an official journal of the American Association for Cancer Research 19 (22) (2013) 6126–6137, https://doi.org/10.1158/1078-0432.CCR-13-0526.

[43] M.A. Nieto, R.Y. Huang, R.A. Jackson, J.P. Thiery, EMT: 2016, Cell 166 (1) (2016) 21–45, https://doi.org/10.1016/j.cell.2016.06.028.

[44] Y.X. Feng, E.S. Sokol, C.A. Del Vecchio, S. Sanduja, J.H. Claessen, T.A. Proia, D.X. Jin, F. Reinhardt, H.L. Ploegh, Q. Wang, P.B. Gupta, Epithelial-to-mesenchymal transition activates PERK-eIF2α and sensitizes cells to endoplasmic reticulum stress, Cancer discovery 4 (6) (2014) 702–715, https://doi.org/10.1158/2159-8290.CD-13-0945.

[45] M.J.P. Crowley, B. Bhinder, G.J. Markowitz, M. Martin, A. Verma, T.A. Sandoval, C.S. Chae, S. Yomtoubian, Y. Hu, S. Chopra, D.A. Tavarez, P. Giovanelli, D. Gao, T.E. McGraw, N.K. Altorki, O. Elemento, J.R. Cubillos-Ruiz, V. Mittal, Tumor-intrinsic IRE1α signaling controls protective immunity in lung cancer, Nat Commun 14 (1) (2023 Jan 9) 120, https://doi.org/10.1038/s41467-022-35584-9.

[46] S.Y. Wang, L.J. Zhang, G.J. Chen, Q.Q. Ni, Y. Huang, D. Zhang, F.Y. Han, W.F. He, L.L. He, Y.Q. Ding, H.L. Jiao, Y.P. Ye, COPA A-to-I RNA editing hijacks endoplasmic reticulum stress to promote metastasis in colorectal cancer, Cancer Lett 553 (2023 Jan 28) 215995, https://doi.org/10.1016/j.canlet.2022.215995. Epub 2022 Nov 4.

[47] C. Salvagno, J.K. Mandula, P.C. Rodriguez, J.R. Cubillos-Ruiz, Decoding endoplasmic reticulum stress signals in cancer cells and antitumor immunity, Trends Cancer 8 (11) (2022 Nov) 930–943, https://doi.org/10.1016/j.trecan.2022.06.006. Epub 2022 Jul 8.

[48] Y. Gu, S. Tang, Z. Wang, L. Cai, H. Lian, Y. Shen, Y. Zhou, A pan-cancer analysis of the prognostic and immunological role of β-actin (ACTB) in human cancers, Bioengineered 12 (1) (2021) 6166–6185, https://doi.org/10.1080/21655979.2021.1973220.

[49] L. Xiao, H. Peng, M. Yan, S. Chen, Silencing *ACTG1* expression induces prostate cancer epithelial mesenchymal transition through *MAPK/ERK* signaling pathway, DNA and cell biology 40 (11) (2021) 1445–1455, https://doi.org/10.1089/dna.2021.0416.

[50] A. Woodward, G.N.F. Faria, R.G. Harrison, Annexin A5 as a targeting agent for cancer treatment, Cancer Lett 547 (2022 Oct 28) 215857, https://doi.org/10.1016/j.canlet.2022.215857. Epub 2022 Aug 6.

[51] B.K. Ahn, S.H. Kim, S.S. Paik, K.H. Lee, Loss of APAF-1 expression is associated with early recurrence in stage I, II, and III colorectal cancer, Langenbecks Arch Surg 401 (8) (2016 Dec) 1203–1210, https://doi.org/10.1007/s00423-016-1483-3. Epub 2016 Aug 2.

[52] Q. Chen, K. Wu, X. Qin, Y. Yu, X. Wang, K. Wei, LASP1 promotes proliferation, metastasis, invasion in head and neck squamous cell carcinoma and through direct interaction with HSPA1A, Journal of cellular and molecular medicine 24 (2) (2020) 1626–1639, https://doi.org/10.1111/jcmm.14854.

[53] B. Wang, T. Lan, H. Xiao, Z.H. Chen, C. Wei, L.F. Chen, J.F. Guan, R.F. Yuan, X. Yu, Z.G. Hu, H.J. Wu, Z. Dai, K. Wang, The expression profiles and prognostic values of HSP70s in hepatocellular carcinoma, Cancer cell international 21 (1) (2021) 286, https://doi.org/10.1186/s12935-021-01987-9.

[54] F. Wang, Y. Qiang, L. Zhu, Y. Jiang, Y. Wang, X. Shao, L. Yin, J. Chen, Z. Chen, MicroRNA-7 downregulates the oncogene VDAC1 to influence hepatocellular carcinoma proliferation and metastasis, Tumour biology 37 (8) (2016) 10235–10246, https://doi.org/10.1007/s13277-016-4836-1.

[55] J. Gao, S. Ma, F. Yang, X. Chen, W. Wang, J. Zhang, Y. Li, T. Wang, L. Shan, miR-193b exhibits mutual interaction with MYC, and suppresses growth and metastasis of osteosarcoma, Oncology reports 44 (1) (2020) 139–155, https://doi.org/10.3892/or.2020.7601.

[56] W. Feng, D.C. Dean, F.J. Hornicek, D. Spentzos, R.M. Hoffman, H. Shi, Z. Duan, Myc is a prognostic biomarker and potential therapeutic target in osteosarcoma, Therapeutic advance es in medical oncology 12 (2020) 1758835920922055, https://doi.org/10.1177/1758835920922055.

[57] H. Song, Y. Zhou, A. Peng, J. Liu, X. Wu, W. Chen, Z. Liu, Aurora-B promotes osteosarcoma cell growth and metastasis through activation of the NPM1/ERK/NF-κβ/MMPs Axis, Cancer management and research 12 (2020) 4817–4827, https://doi.org/10.2147/CMAR.S252847.

[58] S. Zhang, Y. Yang, S. Huang, C. Deng, S. Zhou, J. Yang, Y. Cao, L. Xu, Y. Yuan, J. Yang, G. Chen, L. Zhou, Y. Lv, L. Wang, X. Zou, SIRT1 inhibits gastric cancer proliferation and metastasis via STAT3/MMP-13 signaling, J Cell Physiol 234 (9) (2019 Sep) 15395–15406, https://doi.org/10.1002/jcp.28186. Epub 2019 Feb 2.

[59] D.K. Alves-Fernandes, M.G. Jasiulionis, The role of SIRT1 on DNA damage response and epigenetic alterations in cancer, Int J Mol Sci 20 (13) (2019 Jun 28) 3153, https://doi.org/10.3390/ijms20133153.

[60] A.L.C. Ong, T.S. Ramasamy, Role of Sirtuin1-p53 regulatory axis in aging, cancer and cellular reprogramming, Ageing Res Rev 43 (2018 May) 64–80, https://doi.org/10.1016/j.arr.2018.02.004. Epub 2018 Feb 21.

[61] D.M. Wolf, C. Yau, J. Wulfkuhle, L. Brown-Swigart, R.I. Gallagher, P.R.E. Lee, Z. Zhu, M.J. Magbanua, R. Sayaman, N. O'Grady, A. Basu, A. Delson, J.P. Coppé, R. Lu, J. Braun, I.-S.P.Y.2 Investigators, S.M. Asare, L. Sit, J.B. Matthews, J. Perlmutter, N. Hylton, M.C. Liu, P. Pohlmann, W.F. Symmans, H.S. Rugo, C. Isaacs, A.M. DeMichele, D. Yee, D.A. Berry, L. Pusztai, E.F. Petricoin, G.L. Hirst, L.J. Esserman, L.J. van 't Veer, Redefining breast cancer subtypes to guide treatment prioritization and maximize response: predictive biomarkers across 10 cancer therapies, Cancer Cell 40 (6) (2022 Jun 13) 609–623.e6, https://doi.org/10.1016/j.ccell.2022.05.005. Epub 2022 May 26.